Available online at www.sciencedirect.com
SCIENCE DIRECT
Journal of Catalysis 230 (2005) 14–27
JOURNAL OF CATALYSIS
www.elsevier.com/locate/jcat

Dimethyl carbonate production via the oxidative carbonylation of methanol over Cu/SiO_2 catalysts prepared via molecular precursor grafting and chemical vapor deposition approaches

Ian J. Drake [a], Kyle L. Fujdala [b,c], Alexis T. Bell [a,*], T. Don Tilley [b,c]

[a] *Department of Chemical Engineering, University of California, Berkeley, CA 94720-1462, USA*
[b] *Department of Chemistry, University of California, Berkeley, Berkeley, CA 94720, USA*
[c] *Chemical Sciences Division, Lawrence Berkeley National Laboratory, 1 Cyclotron Road, Berkeley, CA 94720, USA*

Received 27 July 2004; revised 27 September 2004; accepted 1 October 2004

Available online 28 December 2004

Abstract

The influence of catalyst synthesis method and Cu source on the activity and selectivity of Cu/SiO_2 catalysts for the gas-phase oxidative carbonylation of methanol to dimethyl carbonate (DMC) is reported. $[CuOSi(O^tBu)_3]_4$, $[CuO^tBu]_4$, and CuCl were used as precursors to produce highly dispersed silica-supported copper. XANES and EXAFS characterization prior to reaction (but after thermal treatment under He) showed that Cu in the catalysts prepared with CuCl and $[CuOSi(O^tBu)_3]_4$ was present primarily as isolated Cu(I) species, whereas $[CuO^tBu]_4$ produced 1-nm Cu particles. During the catalytic reaction, the Cu in catalysts prepared from CuCl and $[CuOSi(O^tBu)_3]_4$ formed highly dispersed CuO moieties, whereas the Cu in catalysts prepared from $[CuO^tBu]_4$ formed a cuprous oxide layer over a Cu(0) core. For comparison, poorly dispersed Cu on silica was prepared via traditional incipient wetness impregnation with $Cu(NO_3)_2$. It was found that activity for DMC formation increased with increasing Cu dispersion. The selectivity for DMC formation (relative to CO) decreased with decreasing Cu dispersion when the original state of the Cu was Cu(0) directly preceding reaction conditions.

Keywords: DMC synthesis; Oxidative carbonylation; Cu EXAFS; Cu *K*-edge XANES; Cl *K*-edge XANES; Molecular precursor

1. Introduction

Dimethyl carbonate (DMC) has considerable potential as both a chemical intermediate and a fuel additive [1]. It can also be used as a precursor for carbonic acid derivatives and as a methylating agent [2]. Because of its high oxygen content, DMC has been proposed as a replacement for methyl *tert*-butyl ether (MTBE) as a fuel additive [1]. DMC is currently made via the oxidative carbonylation of methanol on unsupported cuprous chloride suspended in a slurry reactor [3]. Since this process suffers from catalyst deactivation, equipment corrosion, and difficulties in product separation, a number of alternative approaches have been investigated. These include cycloaddition of CO_2 to epoxides with the use of titanosilicate molecular sieves [4], various transesterification methods [5,6], methanol carboxylation over zirconia [7–9], and electrochemical oxidative carbonylation of methanol [10,11]. From a thermodynamic standpoint, the oxidative carbonylation of methanol remains the most favorable reaction [1]. To overcome problems with catalyst separation inherent in liquid-phase processes, recent interest has focused on vapor-phase oxidative carbonylation of methanol over supported copper-based catalysts [12–27]. CuCl and $CuCl_2$ supported on activated carbon have been evaluated by a number of groups because of the inherent similarity of such catalysts to those used in the liquid-phase system [12–18]. CuCl, $CuCl_2$, and bimetallic $PdCl_2$-$CuCl_2$ deposited on mesoporous silica supports (HMS silica, MCM-41, and SBA-15) have also been evaluated [20–22]. Addi-

* Corresponding author. Fax: +1 510 642 4778.
E-mail address: bell@cchem.berkeley.edu (A.T. Bell).

0021-9517/$ – see front matter
doi:10.1016/j.jcat.2004.10.001

tional work has been reported on increasing the activity and selectivity of the above-mentioned catalysts by the incorporation of quaternary ammonium salts such as tetrabutylammonium bromide (TBAB) and tetraelthylammonium chloride (TEAC) [22,23]. Finally, Cu-exchanged X and Y zeolites, which are nearly free of chloride ions, have been found to be active for DMC synthesis [24–27]. Although these studies demonstrate the importance of Cu as an essential element, the nature of the active site required to achieve high activity and selectivity is not well understood. In particular, there is little understanding of the oxidation state of Cu and the dispersion of the Cu-containing species under reaction conditions. The aim of the present work was to investigate the performance of well-characterized catalysts prepared by the dispersion of Cu on the mesoporous silica SBA-15. $[CuOSi(O^tBu)_3]_4$, $[CuO^tBu]_4$, and CuCl were used as Cu precursors, since all three were found to produce well-dispersed Cu moieties on SBA-15. XANES and EXAFS were used in situ to follow changes in the oxidation state and structure of the supported Cu.

2. Experimental

2.1. General

All standards and test samples were handled under an inert atmosphere (N_2) in a drybox, with the exception of CuO and $CuCl_2$, which were handled in air. A Quantachrome Autosorb-One was used for N_2 porosimetry measurements. The Brunauer–Emmet–Teller (BET) method [28] was used to determine surface areas, and the Barrett–Joyner–Halenda (BJH) method [29] was used to obtain pore size distributions. The Cu and Cl (where appropriate) contents of the materials studied were determined by Galbraith Laboratories (Knoxville, TN, USA) with ionization-coupled plasma (ICP) methods. $Si(OEt)_4$, Cu_2O, CuO, $Cu(NO_3)_2$, CuCl, $CuCl_2$, and methanol (MeOH) were purchased from Aldrich and used as received. Chlorotriphenylsilane, $ClSi(C_6H_5)_3$, was purchased from Gelest and used as received. Cs_2CuCl_4 was prepared by known literature procedures [30,31]. The mesoporous silica support, SBA-15, was prepared according to literature procedures [32] and characterized by PXRD and N_2 porosimetry (surface area, 894 $m^2\,g^{-1}$; pore volume, 1.13 $cm^3\,g^{-1}$; average pore diameter, 77 Å). The hydroxyl group concentration of the SBA-15 was determined to be 1.3(1) OH nm^{-2}, via reaction of SBA-15 with $Mg(C_6H_5CH_2)_2\cdot 2THF$ and quantification of the toluene evolved by ^1H NMR spectroscopy [33].

2.2. Catalyst preparation

Cu was dispersed onto SBA-15 either by room-temperature grafting of $[CuOSi(O^tBu)_3]_4$ [34] or $[CuO^tBu]_4$ [35], or by reaction of CuCl vapor at elevated temperature. Details of the Cu deposition methods have been described previously [36,37]. After preparation, each catalyst was heated in He at 473 K to remove all organic matter from the samples prepared from either $[CuOSi(O^tBu)_3]_4$ or $[CuO^tBu]_4$, and for consistency for the samples prepared from CuCl. Catalysts prepared from $CuOSi(O^tBu)_3]_4$, $[CuO^tBu]_4$, or CuCl are designated as CuOSi/SBA(x.x), CuO^tBu/SBA(x.x), and CuCl/SBA(x.x), respectively, where x.x indicates the weight loading of Cu determined after He pretreatment by ICP. Designations without the x.x suffix refer to all catalysts of a single Cu precursor. A 5.0 wt% Cu on SBA-15 catalyst was also prepared via aqueous impregnation of $Cu(NO_3)_2$. The freshly impregnated material was dried under ambient conditions, oven dried at 393 K for 5 h, and then calcined in air at 773 K for 2 h. Following calcinations to remove the nitrogen-containing species, the catalyst was reduced in CO at 773 K for 2 h. The reduced catalyst is designated as Cu/SBA(5.0).

2.3. Cu K-edge X-ray absorption spectroscopy (XAS)

EXAFS and XANES data were acquired at the Stanford Synchrotron Radiation Laboratory (SSRL) at Stanford University and at the National Synchrotron Light Source (NSLS) at Brookhaven National Laboratory. Cu *K*-edge absorption measurements were performed on beamline 6-2 at SSRL and on beamline X11A at NSLS. The premonochromator vertical aperture of the beams was set to 0.5 mm for improved resolution, defining an energy resolution of 1.8 eV at the Cu *K*-edge. The monochromator was detuned 20–30% at 400 eV above the Cu *K*-edge. Cu metal foil (7 μm) was used for energy calibration.

Each sample was pressed into a rectangular pellet (0.43×1.86 cm) and loaded into an in situ cell for transmission experiments [38]. A sufficient quantity of each sample was used to give a calculated absorption length ($\mu_m\rho x$) of 2 [39–42]. The cell was evacuated to 10^{-6} Torr, and the sample holder was maintained at 77 K during the experiment. Intensities of the beam were measured over a 900-eV range. The EXAFS region was taken from 30 eV to $12k$ in $0.05k$ steps and from $12k$ to $16k$ in $0.07k$ steps holding for 2 and 3 s, respectively. Ionization chambers (N_2 filled) were used to measure the incident (I_0) and sample transmitted (I_1) fluxes. A third detector (I_2) was used to measure the flux through a (7-μm thick) Cu foil internal standard.

A portable flow manifold was used to treat the catalysts on-site. Each sample was first treated in He (99.999%) at a flow rate of 60 $cm^3\,min^{-1}$. The temperature was increased at 10 K min^{-1} to 573 K and kept isothermal for 2 h to facilitate removal of residual organic species from the grafted materials. This protocol has been shown to be sufficient to remove the organic species. For consistency, this pretreatment was also applied to all CuCl/SBA(x.x) samples. Following pretreatment in He, reaction gases (CO, O_2, MeOH) were introduced into the cell. A $MeOH/O_2/CO/He$ mixture (4.0/1.0/9.0/19.3) was fed to the cell at a nominal total flow

rate of 20 $cm^3\,min^{-1}$. The feed gas was passed over the catalyst for 45 min at 363 K. After this step, the temperature was increased at 10 $K\,min^{-1}$ to 403 K and maintained at this temperature for 1 h. During in situ XANES measurements, scans were taken every 4–6 min.

2.4. Cl *K*-edge X-ray absorption measurements

Cl *K*-edge XANES measurements were performed on beamline 9.3.1 of the Advanced Light Source (ALS) at the Lawrence Berkeley National Laboratory. The beamline has a double-crystal monochromator and was equipped with Si(111) crystals. Focusing optics were present before and after the monochromator. A focused beam spot of approximately 2 mm was measured at the sample. The premonochromator vertical slits were adjusted to define the resolution and flux. The pre-edge feature of $CuCl_2$ was monitored at four different vertical slit separations to optimize the energy resolution. A resolving power of approximately 4000 ($E/\Delta E$) was achieved, which corresponds to approximately 0.5 eV resolution at the Cl *K*-edge. The beamline delivers more than 10^{11} photons s^{-1} between 2500 and 5000 eV. Because the flux drops precipitously above 5000 eV, no detuning of the monochromator was necessary, since the first allowed harmonic occurs above 8000 eV and has a negligible flux. The ALS storage ring operates at 1.9 GeV, and data were taken at a current between 380 and 200 mA.

Samples were loaded on 1 cm × 1 cm plates and loaded into the sample chamber of the end station, which was operated at 10^{-7} Torr. No windows isolated the end station from the beamline in normal operation. A silicon photodiode (Hamamatsu model 3584-02) detector could be maneuvered at a 45° angle relative to the incident radiation within 2–5 mm of the sample face to measure X-ray and visible fluorescence. An electrometer (Keithley 6517A) was used to amplify the photodiode current measurement.

Cl *K*-edge XANES data were collected for standards (CuCl, $CuCl_2$, Cs_2CuCl_4, and $ClSi(C_6H_5)_3$), a sample of newly prepared CuCl/SBA(2.9), and the same material after it had been He pretreated and then exposed to reaction conditions. XANES data were also obtained for SBA-15 that had been impregnated with HCl (from a 0.12 M HCl(aq) solution) and then dried at 393 K for 2 h before heating in a vacuum oven at 423 K for 2 h. A thin pellet of each sample (∼ 15 mg) was pressed and applied to the adhesive side of pre-cut Kapton tape, which was subsequently mounted on the sample holder. All samples were exposed to ambient conditions for ∼ 5 min during transfer from a vial to the sample holder of the end station. Three scans of each standard and five scans of each test sample were measured for an adequate signal-to-noise ratio of the data. The energy was calibrated from the Cl *K*-edge of Cs_2CuCl_4 [43–46]. The maximum of the first edge-region feature in the spectrum was assigned to 2820.20 eV. Scans were made between 2700 and 2923 eV with a 0.1-eV step in the edge region. The reproducibility of the energy is on the order of tens of meV [47]. The CuCl edge did not change over the course of the experiment.

2.5. XANES analyses

Cu and Cl *K*-edge XANES data were analyzed with the WinXAS (v. 2.3) software package [48,49]. The energy was calibrated with the use of the Cu *K*-edge of the Cu foil, which was taken as 8980 eV. Pre-edge absorptions due to the background and detector were subtracted with the use of a linear fit to the data in the range of −200 to −50 eV, relative to the sample edge energy (E_0). Each spectrum was normalized by a constant determined by the average absorption in the range of 100 to 300 eV relative to E_0. The edge energy of each sample and reference was taken at the first inflection point beyond any pre-edge peaks.

Prior to analysis of the Cl *K*-edge data, a linear fit was made to the data in the range of −120 to −20 eV relative to E_0, and this line was subtracted from the data. The spectrum of each sample was normalized by a constant determined by the average absorption in the range of 2840–2860 eV. Energies reported for the inflection point were determined by taking the highest energy maximum in the first derivative of the data in the rising edge region. A pseudo-Voigt line shape set to a fixed 50:50 ratio of Lorentzian–Gaussian contributions was used to model the pre-edge features [43]. The intensity of the pre-edge feature is reported as the peak height multiplied by the full width at half-maximum (FWHM). A detailed error analysis was not pursued.

2.6. EXAFS analyses

Extraction and fitting of the EXAFS function, $\chi(k)$, were done by standard methods with the aid of the UWXAFS [50–52] suite of software programs. We subtracted a background function by taking spline points between k values of 1.5 and 15 $Å^{-1}$. An R_{bkg} value of 1.0 was chosen. Non-phase-corrected Fourier transforms (FT) were performed on the k^3-weighted $\chi(k)$ functions. FT $k^3\chi(k)$ data are plotted without phase correction unless explicitly identified as such. The k range of the transform varied between $k_{min} = 2.0$–3.0 $Å^{-1}$ and $k_{max} = 11.5$–14.0 $Å^{-1}$ for all spectra. The k_{min} and k_{max} values were chosen at node points to help minimize spectral broadening. All spectra were transformed with a Hanning window function with a windowsill (dk) of 1 $Å^{-1}$ centered on the chosen nodal position.

S_0^2 was extracted by fitting the first peak in FT $k^3\chi(k)$ for Cu foil, with the use of the theoretical values of $F_j(k)$ and $\phi_j(k)$ determined by the FEFF8.2 code [53,54]. The fit was done in back FT k-space and in R-space. A value of $S_0^2 = 0.865$ was obtained in both refinements, and this value was used in all subsequent analyses.

All fits of samples and standards were performed on the real and imaginary parts of the FT $k^3\chi(k)$ data. The k and R ranges of all of the sample fits and the number of independent points available to minimize the sum of squares of the

Table 1
k-Space and r-space range for fitting

Catalyst	k_{min} (Å^{-1})	k_{max} (Å^{-1})	Δk	R_{min} (Å)	R_{max} (Å)	ΔR	N_{ind}[a]
CuCl/SBA(2.9)	2.2	11.0	8.8	1.2	3.0	1.8	12.1
CuOSi/SBA(3.6)	2.9	12.3	9.4	1.2	3.0	1.8	12.8
CuO^{t}Bu/SBA(3.4)	3.0	12.8	9.8	1.1	3.0	1.9	13.9

[a] Number of independent data points (N_{ind}) in fit calculated by $N_{ind} = 2(\Delta k)(\Delta R)/\pi + 2$.

difference between the model and $\chi(k)$ data are listed in Table 1. Two to three shells were fit simultaneously, allowing σ, R_j, and N_j to be adjusted for each Fourier component. A single edge shift correction (ΔE_0) was refined for each fit, unless reported otherwise. The quality of a particular fit was evaluated by use of the reduced chi-square method (χ^2_ν) [55]. Once a best fit was found, the $\Re$-factor was recorded for presentation of the fits. This factor gives a sum-of-square measure of the fractional misfit [55]. More extensive details of the EXAFS analysis performed in this work, including details of the phase and amplitude functions used in the fits, can be found elsewhere [36,37].

2.7. Studies of catalytic activity and selectivity

Catalyst (150 mg) (typically 1.2 cm^3) was loaded into a 10-mm-diameter tubular flow reactor made of Pyrex. A glass frit fused inside the reactor was used to support the catalyst. The reactor was heated in a tubular furnace. The reactor thermocouple and a pressure transducer, multiple solenoid valves, and all system thermocouples were interfaced to a personal computer via an analog-to-digital/digital-to-analog board (NI PCI-6052E). A LabVIEW program was developed to monitor and control the reactor temperature and the pressure in the reactor and to switch gases. Each catalyst was pretreated at 573 K for 1 h in a stream of high-purity He (99.999%). For the catalytic experiment, CO (99.9%, 0.1% Ar), O_2 (20.0%, 80.0% He), and He (99.999%) were used together with methanol (MeOH), which was introduced by passage of the He carrier gas through a saturator maintained at 306 K. CO, O_2, and the MeOH-saturated He stream were mixed in a mixing volume filled with 1.0-mm quartz beads before they were passed into the reactor. A MeOH/O_2/CO/He mixture (4.0/1.0/9.0/19.3) was fed to the reactor at a nominal total flow rate of 20 cm^3 min^{-1}, which was varied between 10 and 40 cm^3 min^{-1} to study the effect of residence time. The feed gas was passed over the catalyst for 45 min at 363 K. After this step, the temperature was increased at 10 K min^{-1} and held constant in 10 K increments between 383 and 423 K. Following reaction at 423 K, the reactor was cooled to 393 K to check the reproducibility of catalyst performance. All lines were heated to avoid condensation of methanol and products. The product stream was analyzed by a gas chromatograph (GC) (Agilent 6890) equipped with a capillary column (Alltech, AT aquawax; polyethylene glycol stationary phase) connected to a flame ionization detector (FID) and by a packed column (Alltech, Haysep DB packing) connected to a thermal conductivity detector (TCD). Oxygenated compounds (MeOH, methyl formate, dimethoxymethane, dimethyl ether, and formaldehyde) were detected with the FID, whereas fixed gases (CO, O_2, CO_2) were detected with the TCD. Complete GC product analysis run time was ca. 30 min. Three points were taken at each temperature or residence time and checked for reproducibility.

3. Results

3.1. General

The surface area and pore volume of freshly prepared CuOSi/SBA(3.6) (678 m^2 g^{-1} and 0.88 cm^3 g^{-1}) were lower than those of SBA-15 (894 m^2 g^{-1} and 1.13 cm^3 g^{-1}). However, after heating at 673 K under flowing N_2 (to remove the organic species), the surface area and pore volume of CuOSi/SBA(3.6) increased (800 m^2 g^{-1} and 1.01 cm^3 g^{-1}), indicating that pore filling by the bulky molecular precursor is responsible for the initial decreases. Similar behavior was observed for CuOSi/SBA(5.2), CuO^{t}Bu/SBA(3.4), and CuO^{t}Bu/SBA(4.3) [56].

Reaction of SBA-15 with varying amounts of CuCl at 873 K produced a light yellow powder for all Cu loadings. The surface area and pore volume of freshly prepared CuCl/SBA(2.9) (590 m^2 g^{-1} and 0.76 cm^3 g^{-1}) were lower than the values found for the SBA-15 support (894 m^2 g^{-1} and 1.13 cm^3 g^{-1}), indicative of pore collapse during the catalyst preparation. Helium pretreatment and exposure to reaction conditions did not affect the surface area or pore volume of any catalysts studied.

Table 2 lists the actual and targeted Cu contents for each of the catalysts. It is evident that using [CuO^{t}Bu]$_4$ or [CuOSi(O^{t}Bu)$_3$]$_4$ as the Cu source provides Cu loadings close to the targeted values. In contrast, using CuCl led to divergence of the targeted and actual Cu loadings with increasing Cu loading. These data indicate that Cu deposition using the low-temperature grafting of [CuO^{t}Bu]$_4$ and [CuOSi(O^{t}Bu)$_3$]$_4$ is much more efficient when compared with high-temperature CVD using CuCl. For example, only a Cu loading of 2.92% could be achieved despite the use of sufficient CuCl for a Cu loading of 7%. Furthermore, use of CuCl introduced Cl into the final catalyst (between 0.1 and 0.35% as the Cu loading increased from 1.1 to 2.9%).

3.2. Catalytic performance

The activities of CuCl/SBA(2.9), CuOSi/SBA(3.6), and CuO^{t}Bu/SBA(3.4) were compared at a constant reactor residence time of 3.5 s for temperatures between 383 and 423 K. The only products observed were DMC, methyl formate (MF), and CO_2. Fig. 1 presents the DMC, MF, and CO_2 activities of each catalyst reported as an apparent turnover

Table 2
Materials analysis

Catalyst ID	Preparation method	Cu (wt%)	Targeted Cu (wt%)	Before reaction		After reaction	
				Cl (wt%)	Cu/Cl (atom)	Cu (nm^2)	Cl (wt%)
CuCl/SBA(1.1)	CuCl sublimation	1.14	1.5	0.08	7.8	0.14	0.10
CuCl/SBA(2.2)		2.17	3.5	0.18	6.7	0.26	0.18
CuCl/SBA(2.9)		2.92	7.0	0.35	4.7	0.35	0.33
CuOSi/SBA(1.4)	Non-aqueous grafting	1.44	1.5	–	–	0.17	
CuOSi/SBA(3.6)		3.61	3.5	–	–	0.43	
CuOSi/SBA(5.2)		5.21	5.0	–	–	0.62	
CuO^{t}Bu/SBA(1.4)	Non-aqueous grafting	1.37	1.5	–	–	0.16	
CuO^{t}Bu/SBA(3.4)		3.35	3.5	–	–	0.40	
CuO^{t}Bu/SBA(4.3)		4.31	5.0	–	–	0.51	

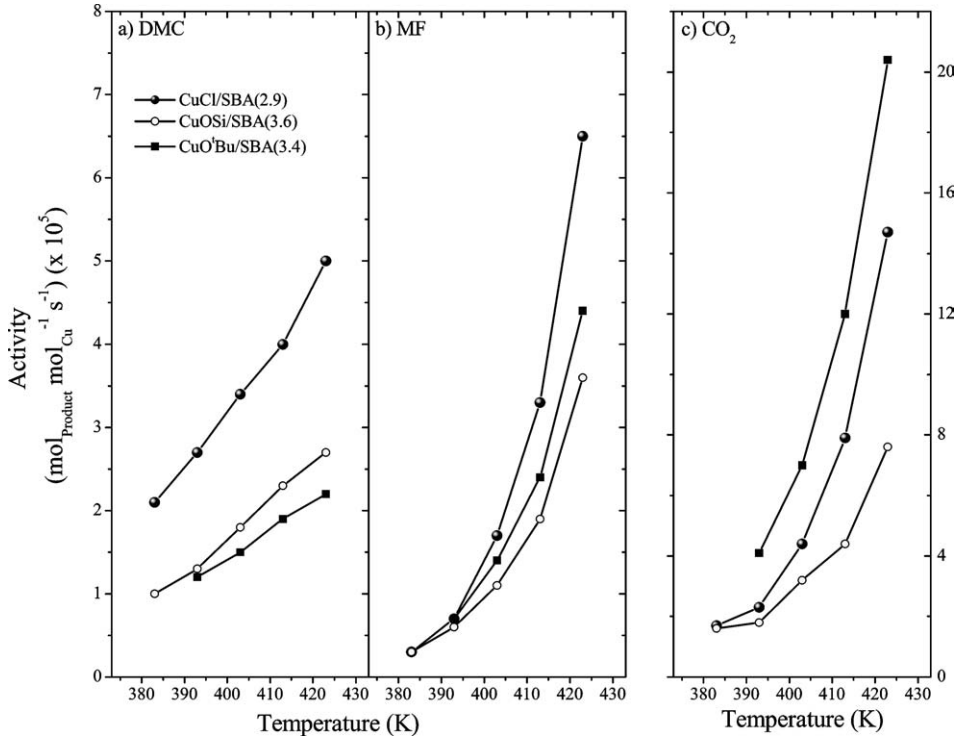

Fig. 1. Effect of precursor composition on catalyst activity. Catalysts are compared at a constant residence time of 3.5 s. Rates of (a) DMC, (b) MF, and (c) CO_2 production. Reaction conditions: MeOH/O_2/CO/He gas mixture (4.0/1.0/9.0/19.3) was fed to the reactor at a nominal total flow rate of 20 cm^3 min^{-1}.

frequency (TOF) normalized to the total number of moles of Cu reported from data in Table 2. The DMC activity decreases in the order CuCl/SBA(2.9) > CuOSi/SBA(3.6) > CuO^{t}Bu/SBA(3.4), whereas the MF activity decreases in the order CuCl/SBA(2.9) > CuO^{t}Bu/SBA(3.4) > CuOSi/SBA(3.6). The rate of CO_2 production decreases in the order CuO^{t}Bu/SBA(3.4) > CuCl/SBA(2.9) > CuOSi/SBA(3.6). DMC selectivity is reported on the basis of methanol consumption ($S_{DMC/MeOH}$) and on the basis of CO consumption ($S_{DMC/CO}$). The CO_2 formed is attributed exclusively to CO oxidation, since over the temperature range investigated no evidence was found for the combustion of methanol or products derived from methanol. CuCl/SBA(2.9) exhibits the highest values of $S_{DMC/MeOH}$ and $S_{DMC/CO}$ at each temperature. The values of $S_{DMC/MeOH}$ and $S_{DMC/CO}$ for CuOSi/SBA(3.6) approached those of CuCl/SBA(2.9) with increasing temperature. CuO^{t}Bu/SBA(3.4) was the least selective catalyst for DMC formation from both methanol and CO.

Table 3 lists the apparent activation energies (E_{app}) based on the data in Fig. 1. The values of E_{app} for DMC for CuCl/SBA(2.9), CuOSi/SBA(3.6), and CuO^{t}Bu/SBA(3.4) are 30, 34, and 25 kJ/mol, respectively. Whereas E_{app} for DMC does not vary significantly, larger differences are seen in E_{app} for MF and CO_2. The values of E_{app} for MF for CuCl/SBA(2.9), CuOSi/SBA(3.6), and CuO^{t}Bu/SBA(3.4) are 102, 80, and 90 kJ/mol, respectively. Last, the values of E_{app} for CO_2 for CuCl/SBA(2.9), CuOSi/SBA(3.6), and CuO^{t}Bu/SBA(3.4) are 72, 53, and 71 kJ/mol, respectively.

The effects of Cu weight loading were investigated at 403 K for a constant residence time of 3.5 s. Turnover frequencies and DMC selectivities are presented in Table 4. As the Cu loading for CuCl/SBA increases from 1.1 to 2.9 wt%, the DMC turnover frequency calculated on a total copper basis stays nearly constant (3.5 s^{-1}). Over the same range of Cu loadings, the TOFs for CO_2 and MF formation remain essentially constant. DMC selectivities are shown for residence times of 3.5 and 0 s. The latter value was obtained by the extrapolation of data taken as a function of residence time and represents the intrinsic selectivity exclusive of secondary reactions. The values of $S^{o}_{DMC/CO}$ and $S^{o}_{DMC/MeOH}$ for CuCl/SBA show little dependence on Cu loading. In all cases, the intrinsic selectivity for DMC from methanol is very high, reaching a maximum value of 90%, whereas the selectivity to DMC from CO is only slightly higher than 50%. Similar patterns are observed in the activity and selectivity of CuOSi/SBA for Cu weight loadings of 1.4, 3.6, and 5.2 wt%. For these catalysts, the intrinsic selectivity for DMC from methanol does not exceed 83%, but the intrinsic selectivity for DMC from CO is again near 50%.

Table 3
Apparent activation energies for CuCl/SBA(2.9), CuOSi/SBA(3.6), and CuO^{t}Bu/SBA(3.4)

Catalyst	E_{app}		
	DMC (kJ/mol)	MF (kJ/mol)	CO_2 (kJ/mol)
CuCl/SBA(2.9)	30 ± 2[a]	102 ± 5	72 ± 3
CuOSi/SBA(3.6)	34 ± 2	80 ± 1	53 ± 5
CuO^{t}Bu/SBA(3.4)	25 ± 1	80 ± 4	71 ± 5

[a] Δt_{95} error calculated using Arrhenius plots at three to four different residence times.

Three CuO^{t}Bu/SBA catalysts were also studied, with Cu loadings of 1.4, 3.4, and 4.3 wt%. The DMC activities of these catalysts based upon the total Cu content of each catalyst are very similar to those of CuOSi/SBA, and both sets of catalyst show a modest decrease in DMC TOF with increasing Cu loading. The MF TOFs calculated on a total Cu basis are also very similar for the CuOSi/SBA and CuO^{t}Bu/SBA catalysts. A significant difference between all of the catalysts is that the CO_2 TOF is much higher for CuO^{t}Bu/SBA than for either CuOSi/SBA or CuCl/SBA. Consistent with

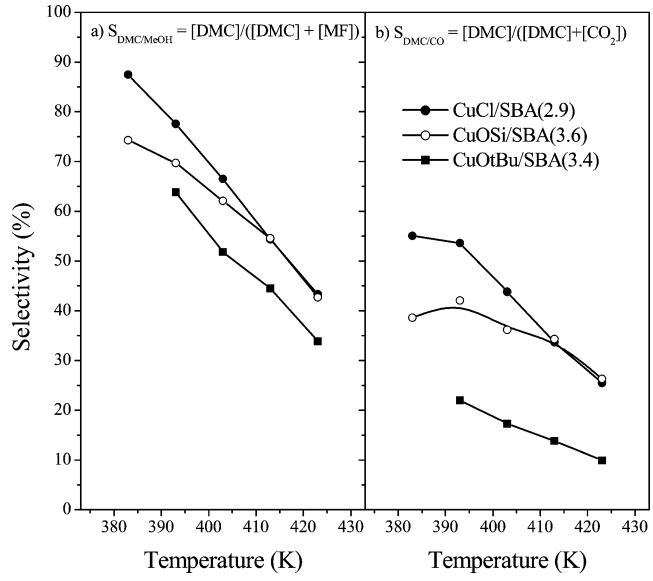

Fig. 2. Effect of catalyst composition on catalyst selectivity. Catalysts are compared at a constant residence time of 3.5 s. (a) $S_{DMC/MeOH}$, (b) $S_{DMC/CO}$. Reaction conditions: MeOH/O_2/CO/He gas mixture (4.0/1.0/9.0/19.3) was fed to the reactor at a nominal total flow rate of 20 cm^3 min^{-1}.

Table 4
Performance comparison for all catalysts as a function of copper loading at 403 K

Catalyst[a]	$S_{DMC/CO}$[b]	$S^{o}_{DMC/CO}$[c]	$S_{DMC/MeOH}$[d]	$S^{o}_{DMC/MeOH}$[e]	$TOF_{product}$[f] ($mol_{product}$ mol^{-1}_{Cu} s^{-1}) ($\times 10^5$)		
					DMC	MF	CO_2
CuCl/SBA(1.1)	48.8	52.0	80.1	90.0	3.5	0.9	3.6
CuCl/SBA(2.2)	47.6	58.7	69.7	85.5	3.5	1.5	3.8
CuCl/SBA(2.9)	43.8	55.4	66.5	83.3	3.3	1.6	4.2
CuOSi/SBA(1.4)	38.2	44.2	71.4	82.9	2.1	0.8	3.4
CuOSi/SBA(3.6)	36.2	49.5	62.1	79.4	1.7	1.1	3.0
CuOSi/SBA(5.2)	34.5	49.5	52.3	72.7	1.5	1.4	2.8
CuO^{t}Bu/SBA(1.4)	17.9	22.3	65.9	80.5	2.0	1.1	9.3
CuO^{t}Bu/SBA(3.4)[g]	18.3	–	51.8	–	1.5	1.4	6.5
CuO^{t}Bu/SBA(4.3)	14.5	18.3	51.9	67.0	1.3	1.2	7.8
Cu/SBA(5.0)	7.3	10.0	37.3	52.0	0.8	1.5	11.0

[a] Reaction temperature, 403 K; CO, 0.27 atm; MeOH, 0.12 atm; O_2, 0.03 atm; residence time, 3.5 s.
[b] $S_{DMC/CO} = [DMC]/([DMC] + [CO_2])$.
[c] $S^{o}_{DMC/CO}$ is the selectivity extrapolated to zero residence time.
[d] $S_{DMC/MeOH} = [DMC]/([DMC] + [MF])$.
[e] $S^{o}_{DMC/MeOH}$ is the selectivity extrapolated to zero residence time.
[f] TOF is reported on the basis of total Cu.
[g] $S^{o}_{DMC/MeOH}$ and $S^{o}_{DMC/CO}$ are not reported because the residence time was not varied.

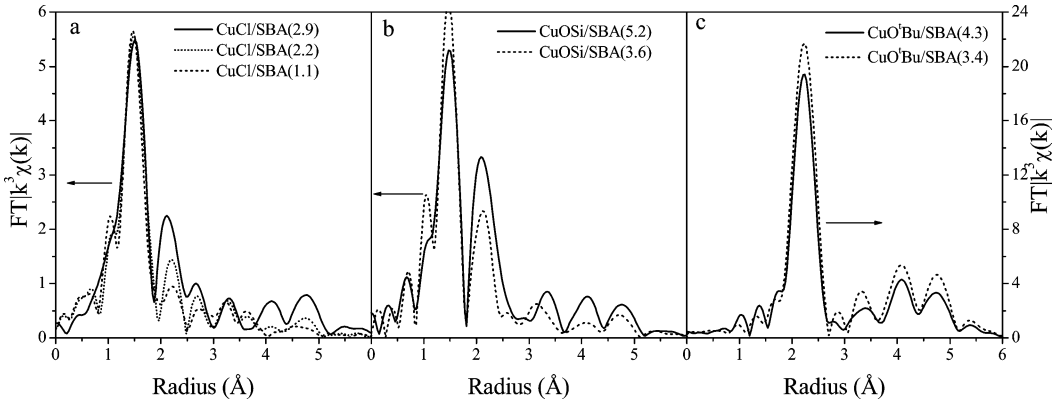

Fig. 3. Fourier transformed $k^3\chi(k)$ (non-phase corrected) for (a) CuCl/SBA(2.9), CuCl/SBA(2.2), and CuCl/SBA(1.1); (b) CuOSi/SBA(5.2) and CuOSi/SBA(3.6); (c) CuO^{t}Bu/SBA(4.3) and CuO^{t}Bu/SBA(3.4). Catalysts were pretreated in He at 573 K prior to EXAFS analysis.

the above observations, the values of $S^{o}_{DMC/CO}$ are significantly lower for CuO^{t}Bu/SBA catalysts when compared with those for the other two sets of catalysts; however, the values of $S^{o}_{DMC/MeOH}$ remain relatively high, although they are still lower than those for CuCl/SBA and CuOSi/SBA.

Cu/SBA(5.0), prepared via the incipient wetness impregnation of SBA-15 with the use of $Cu(NO_3)_2$, followed by reduction in CO at 773 K for 2 h, was also studied. This catalyst was the most active for MF and CO_2 production and the least active for DMC formation. Consequently, this catalyst was the least selective for DMC production from CO consumption, approaching only 10.0% at zero conversion. Likewise, $S^{o}_{DMC/MeOH}$ was only 52.0% at zero conversion.

3.3. Catalyst characterization

3.3.1. EXAFS of pretreated catalysts

FT $k^3\chi(k)$ spectra of CuCl/SBA(2.9), CuCl/SBA(2.2), CuCl/SBA(1.1), CuOSi/SBA(5.2), CuOSi/SBA(3.6), CuO^{t}Bu/SBA(4.3), and CuO^{t}Bu/SBA(3.4) taken after He pretreatment at 573 K are shown in Fig. 3. Detailed discussion of these spectra has previously been presented [36]; hence only a brief summary is presented here. The FT $k^3\chi(k)$ spectra for both CuO^{t}Bu/SBA(3.4) and CuO^{t}Bu/SBA(4.3) (Fig. 3c) have characteristics resembling those of Cu foil (not shown). The peaks at 2.23, 3.4, 4.1, and 4.7 Å (non-phase-corrected) represent the first four coordination shells of Cu in Cu metal. Combined with the absence of any significant Fourier component that can be assigned to Cu–O backscattering, this suggests that all Cu has been reduced to Cu metal. A complete FEFF simulation of CuO^{t}Bu/SBA(3.4) and CuO^{t}Bu/SBA(4.3) was performed, assuming that the observed FT $k^3\chi(k)$ spectra represent the average scattering of a single Cu atom in a 7-Å-diameter cuboctahedron [36,37]. Close agreement between simulation and experiment suggests that Cu in the as-prepared material undergoes reduction and sintering during He pretreatment. By contrast, the FT $k^3\chi(k)$ spectra of CuOSi/SBA(3.6) and CuOSi/SBA(5.2) (Fig. 3b) show a prominent Fourier component at 1.47 Å that can be assigned to Cu–O backscattering, suggesting that the dominant sites are still Cu(I) species associated with O [35–37]. The FT $k^3\chi(k)$ spectra of CuOSi/SBA(3.6) and CuOSi/SBA(5.2) also exhibit peaks at 2.11, 3.34, 4.1, and 4.7 Å (associated with Cu metal), but they are significantly smaller in magnitude than those observed in the spectra of CuO^{t}Bu/SBA(3.4) and CuO^{t}Bu/SBA(4.3). Suggesting the presence of only minor amounts of Cu metal. The FT $k^3\chi(k)$ spectra of CuCl/SBA(2.9), CuCl/SBA(2.2), and CuCl/SBA(1.1) after He pretreatment at 573 K for 1 h (Fig. 3a) are quite similar to those of CuOSi/SBA(3.6) and CuOSi/SBA(5.2), suggesting that the primary sites contain Cu(I) species associated with O atoms, and that only a small fraction of Cu is in a metallic state [36]. The spectra presented in Figs. 3a and b are well represented by a linear combination of the experimental $k^3\chi(k)$ and FT $k^3\chi(k)$ data for He-treated (573 K) CuO^{t}Bu/SBA(3.4) with freshly prepared (not shown, refer to [37]) CuCl/SBA(2.9), CuCl/SBA(2.2), and CuCl/SBA(1.1) and CuOSi/SBA(5.2), CuOSi/SBA(3.6), and CuOSi/SBA(1.4), respectively, which contain only isolated Cu(I) species [36,37]. Table 5 shows the fraction of Cu present as small crystallites following He pretreatment at 573 K for each of the catalysts. Also listed is the fraction of the Cu available for catalysis. It is apparent that more than 91% of the Cu present on CuCl/SBA and CuOSi/SBA is available for catalysis, but that only 58% of the Cu is available for catalysis on CuO^{t}Bu/SBA.

Fig. 4 shows normalized absorption and first-derivative spectra for selected standards. Edge energies (E_0) obtained from the XANES spectra of the standards are listed in Table 6. The values of E_0 for Cu(0) (based on Cu foil), Cu(I) (based on Cu_2O), and Cu(II) (based on CuO) are 8980.0 eV, 8980.8 eV, and 8984.5 (eV), respectively. Although E_0 for Cu_2O is very close to that of metallic Cu, it lies within the range of values reported for Cu(I) compounds, 8980.8 and 8982.8 eV [37]. In situ XANES of CuCl/SBA(2.9), CuSiO/SBA(3.6), and CuO^{t}Bu/BA(3.4) were recorded to determine the change in oxidation state of each catalyst upon exposure of the He-pretreated catalyst to the feed gas mixture at 363 K. The temporal changes in the normalized ab-

Table 5
Fraction of Cu present as metallic Cu crystallites after He pretreatment and the dispersion of Cu determined by EXAFS analysis

Sample	X_{Fresh} [a]	X_{Metal} [b]	Dispersion[c] (%)
CuO^{t}Bu/SBA(3.4)	0.000	1.000	58.1
CuO^{t}Bu/SBA(4.3)	0.000	1.000	58.1
CuOSi/SBA(3.6)	0.880	0.120	94.9
CuOSi/SBA(5.2)	0.785	0.215	91.0
CuCl/SBA(1.1)	0.980	0.020	99.2
CuCl/SBA(2.2)	0.926	0.074	96.9
CuCl/SBA(2.9)	0.893	0.107	95.5
Cu/SBA(5.0)	0.000	1.000	5[d]

[a] Fraction of total Cu present as Cu metal in the freshly prepared sample.
[b] Fraction of total Cu present as Cu metal after He pretreatment. Particles of Cu are taken to be 55 atom cluster (fcc with corners removed) [36].
[c] Fraction of Cu sites in contact with the gas phase.
[d] Estimated dispersion determined by Scherrer analysis of the Cu(111) diffraction peak [61]. The particles are estimated to be 300 Å in diameter.

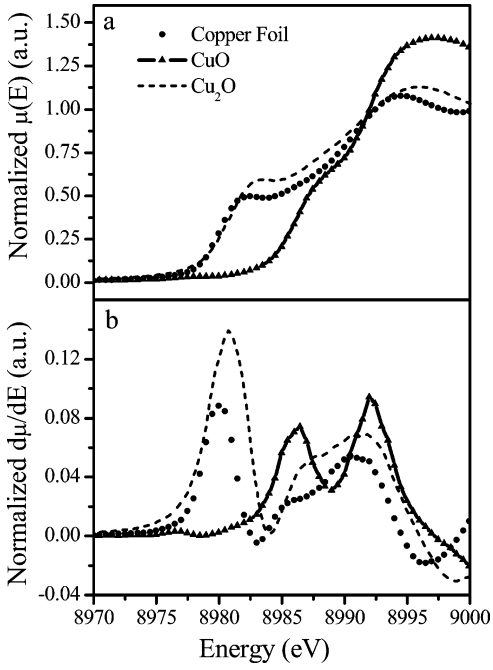

Fig. 4. Cu K-edge XANES spectra of standards. (a) Normalized absorption spectra of Cu^0 (Cu foil), Cu(I) (Cu_2O), and Cu(II) (CuO) standards. (b) First derivative spectra of (a).

sorption and first-derivative spectra of CuCl/SBA(2.9), CuSiO/SBA(3.6), and CuO^{t}Bu/BA(3.4) over a 30-min period are shown in Fig. 5, and the measured edge features are listed in Table 6. At $t = 0$ min, the absorption spectra of CuCl/SBA(2.9) and CuOSi/SBA(3.6) exhibit a single inflection point, which occurs at 8981.5 for CuCl/SBA(2.9) and at 8982.0 for CuOSi/SBA(3.6), corresponding to the Cu(I) oxidation state. There is no indication of an inflection point at ca. 8985 eV corresponding to Cu(II). The absorption spectrum of CuO^{t}Bu/SBA(3.4) also exhibits a single inflection point at $t = 0$ min. However, this inflection point at 8980.4 corresponds to the Cu(0) state, consistent with the EXAFS analysis above.

Table 6
XANES edge-energies for samples under reaction conditions compared to standards

Sample	Formal valency	E_0 (eV)	
		First inflection[a]	Second inflection[b]
Cu foil	0	8980.0	–
[CuOSi[O^{t}Bu]$_3$]$_4$[c]	1	8982.1	–
[CuO^{t}Bu]$_4$[c]	1	8981.5	–
CuCl[c]	1	8982.8	–
Cu_2O	1	8980.8	–
CuO	2	8984.5	–
CuCl/SBA(2.9), $t = 0$ min	1	8981.5	–
CuCl/SBA(2.9), $t = 30$ min	–	8981.5	8985.4
CuOSi/SBA(3.6), $t = 0$ min	1	8982.0	–
CuOSi/SBA(3.6), $t = 30$ min	–	8981.5	8986
CuO^{t}Bu/SBA(3.4), $t = 0$ min	0	8980.4	–
CuO^{t}Bu/SBA(3.4), $t = 30$ min	1	8981.3	–

[a] Based on the first inflection point corresponding to a shoulder of peak on the rising absorption edge.
[b] Based on the second inflection point corresponding to a shoulder or peak on the rising absorption edge.
[c] Refs. [36,37].

Following exposure of the catalyst to the reaction feed gas mixture, changes occurred in the spectrum of each catalyst at 363 K. The normalized first-derivative spectra of CuCl/SBA(2.9) shows a decrease in the peak centered at 8981.5 eV (Cu(I)) and an increase in a second peak centered at 8985.4 eV (Cu(II)). Similarly, the normalized first-derivative spectrum of CuOSi/SBA(3.6) shows a corresponding decrease in the first peak centered at 8981.5 eV and an increase in a second peak centered at 8986.0 eV. Finally, CuO^{t}Bu/SBA(3.4) shows a 1.0-eV shift in the first inflection point with an increase in the derivative intensity. With time, the peak at 8981.3 decreases slightly, and only a very small peak at 8986.0 eV is observed. The first of these peaks is clearly identified with Cu(I) species, whereas the second is probably due to a small concentration of Cu(II) species. The in situ spectra of CuCl/SBA(2.9) and CuSiO/SBA(3.6) exhibit edge energies at 8981.4 eV and 8985.4 eV, and 8982.0 eV and 8986.4 eV, respectively. The lower of the two values of E_0 lies in the range characteristic of Cu(I), whereas the higher value of E_0 is characteristic of Cu(II). The fraction of Cu present as Cu(I) increases in the order CuOSi/SBA(3.6) $\sim$ CuCl/SBA(2.9) $<$ CuO^{t}Bu/SBA(3.4). With increasing reaction temperature the fraction of Cu(I) in CuCl/SBA(2.9) increased slightly over that in CuOSi/SBA(3.6).

As reported in Table 2, all of the CuCl/SBA catalysts contained residual Cl species. The nature of the Cl on the surface of CuCl/SBA(2.9) was investigated by Cl K-edge XANES (Fig. 6), since this technique is known to be a direct probe of Cu–Cl bonding [43–45,57–59]. After treatment in reaction conditions, CuCl/SBA(2.9) exhibits a pre-edge feature at 2822.5 eV, a shoulder/edge peak at 2823.8 eV, and a rising edge inflection point at 2825.3 eV. Although the first of

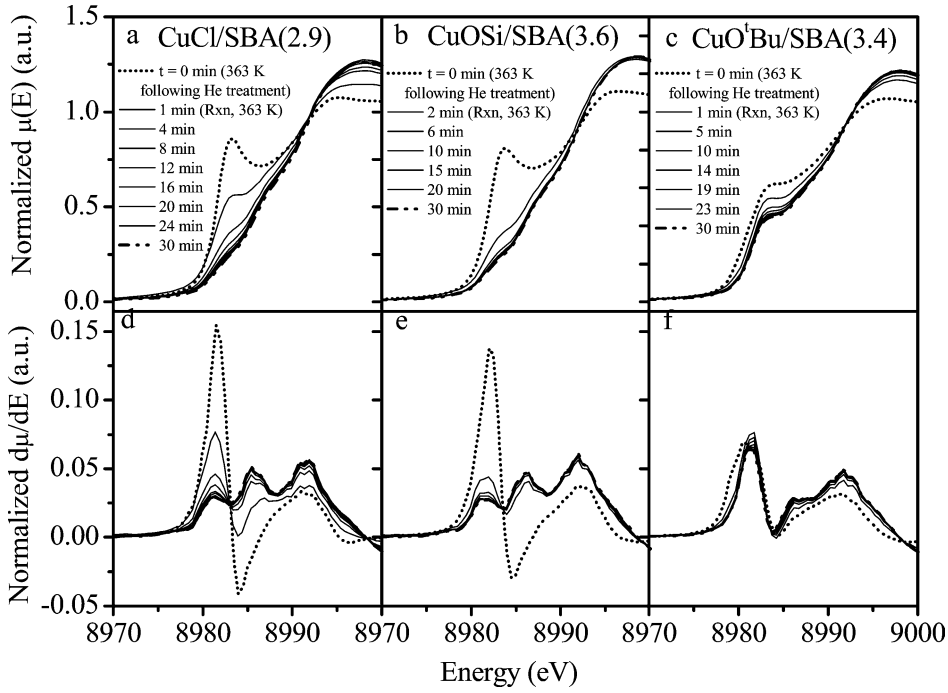

Fig. 5. Normalized absorption and first derivative spectra of transient change in XANES spectra: CuCl/SBA(2.9) (a,d), CuOSi/SBA(3.6) (b,e), and CuO^{t}Bu/SBA(3.4) (c,f) during first contact of reaction gas flow at 363 K. MeOH/O_2/CO/He gas mixture (4.0/1.0/9.0/19.3) was fed to the in situ cell at a nominal total flow rate of 20 cm^3 min^{-1}.

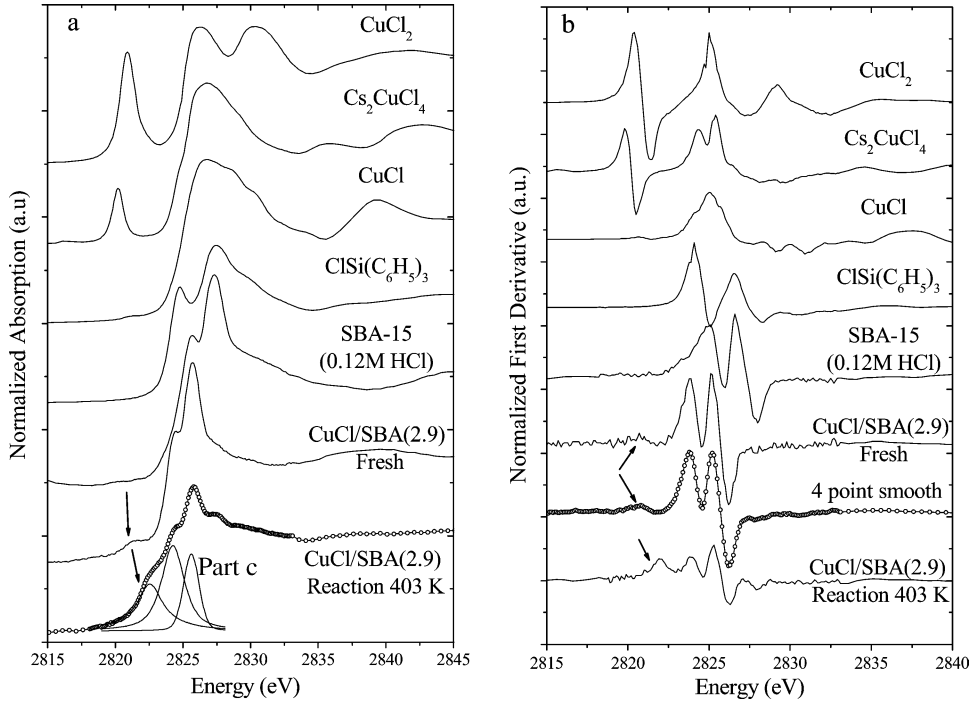

Fig. 6. Cl K-edge XANES spectra of standards and catalysts. Normalized (a) absorption and (b) first derivative spectra. A four point smoothing is shown for the first derivative spectrum of CuCl/SBA(2.9) to accentuate pre-edge inflection point indicated by arrow. (c) Deconvolution of the normalized absorption spectrum of CuCl/SBA(2.9) after reaction conditions at 403 K. The absorption edge was simulated by a pseudo-Voigt fit.

these features is 1.6 eV above that for $CuCl_2$ (2820.9 eV), it lies well within the range of pre-edge energies reported previously for tetrahedral metal chlorides [56]. Association of Cl with a Cu in a formal +2 state is consistent with the Cu XANES spectrum of CuCl/SBA(2.9) taken after treatment in reaction conditions. The shoulder/edge peak at 2823.8 eV may be due to Cl atoms bonded to the support via Si–Cl bonds. This interpretation is suggested by the similarity of

the position of this peak to that observed for HCl-treated SBA-15 (2825.1 eV) and $ClSi(C_6H_5)_3$ (2824.1 eV). All relevant spectral features are summarized in Table 6.

In situ FT $k^3\chi(k)$ and $k^3\chi(k)$ spectra for CuCl/SBA(2.9), CuOSi/SBA(3.6), and CuO^{t}Bu/SBA(3.4) are shown in Fig. 7 together with their respective fits in R-space. The fitted EXAFS parameters for specific atom pairs are given in Table 7. CuCl/SBA(2.9) and CuOSi/SBA(3.6) exhibit similar spectra; both having a non-phase-corrected Fourier component centered at 1.53 Å attributed to oxygen backscattering [36] and a second, non-phase-corrected Fourier component centered at 2.63 Å. To identify the backscatterer responsible for this latter peak, a phase and amplitude correction was applied according to Eq. (1). In the equation

$$F'(R) = \int_{k1}^{k2} k^3 w(k)\chi(k)e^{-\phi(k)}e^{ir}\,dk, \qquad (1)$$

$w(k)$ is the Hanning apodization function, $\phi(k)$ is the phase function, and all other terms are as defined previously. Phase and amplitude functions associated with Si and Cu backscattering were considered. Based upon the Lee and Beni criteria [60] for determination of a specific backscattering pair, the second Fourier component could be assigned to Cu–Cu backscattering. The Cu–Cu phase-corrected spectrum for CuCl/SBA(2.9) after reaction conditions at 403 K is shown in Fig. 8. The Fourier component is symmetrical, and the peak in the magnitude corresponds to the peak in the imaginary part of the magnitude function, proving its proper identification as a Cu–Cu backscattering contribution. This technique was also applied to CuOSi/SBA(3.6) with identical results.

The bond distances determined for CuCl/SBA(2.9) and CuOSi/SBA(3.6) by fitting of the Cu–O and Cu–Cu shells to theoretical scattering pairs ($R_{Cu–O} \sim 1.94$ Å, $R_{Cu–Cu} \sim 2.93$ Å, respectively) agree closely with the bond distances characteristic of crystalline CuO ($R_{Cu–O} \sim 1.95$ Å, $R_{Cu–Cu} \sim 2.90$ Å). The absence of Fourier components beyond 3 Å suggests that there is no long-range ordering and, hence, that the CuO species are small and amorphous. The Cu–Cu and Cu–O coordination numbers were larger for CuOSi/SBA(3.6) (2.3(8) and 3.4(2), respectively) compared

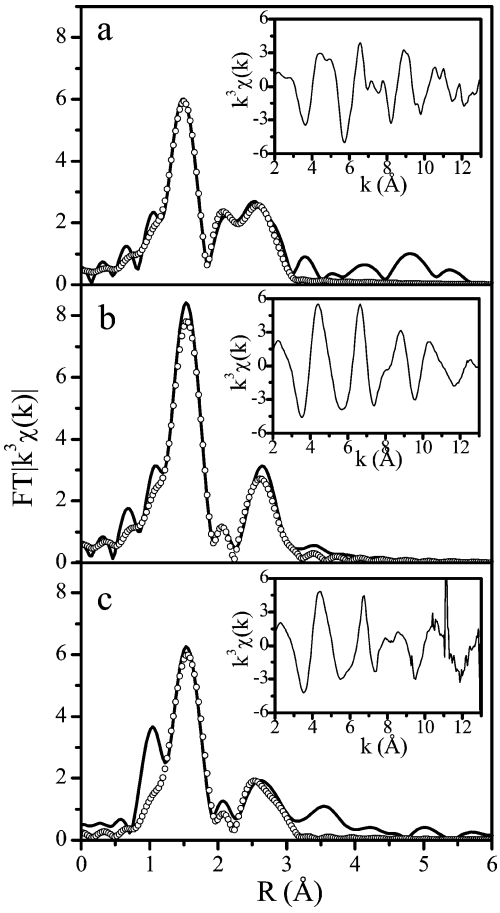

Fig. 7. Fourier transformed $k^3\chi(k)$ and the fitting results for the catalysts after reaction conditions of 20% CO, 2% O_2 and 10% MeOH at 403 K: (a) CuO^{t}Bu/SBA(3.4), (b) CuOSi/SBA(3.6), (c) CuCl/SBA(2.1). The fits are indicated by open circles. The inset of each respective spectrum shows the corresponding $k^3\chi(k)$ used for the Fourier transform.

Table 7
Cl K-edge spectral analysis

Sample	Pre-edge energy[a] (eV)	Normalized pre-edge intensity[d] (eV)	Shoulder/edge-peak inflection point[e] (eV)	Rising edge inflection point[f] (eV)	Coordination charge (η)[g]
$CuCl_2$	2820.9	1.47	2824.7	2825.0	−0.65
Cs_2CuCl_4	2820.2	0.51	2824.3	2825.4	−0.52
CuCl	2821.6[b]	0.05	–	2825.0	−0.65
$ClSi(C_6H_5)_3$	–	–	2824.1	2826.6	−0.13
SBA-15 (0.12 M HCl)	–	–	2825.1	2826.6	−0.13
CuCl/SBA(2.9) Fresh	2821.7	0.11	2823.9	2825.1	−0.62
CuCl/SBA(2.9) Rxn	2822.5[c]	0.48	2823.8	2825.3	−0.56

[a] Maximum in the first edge-region feature in the spectrum.
[b] Not expected since Cu(I) is d^{10}. Suggests slight Cu(II) contamination.
[c] A pseudo-Voigts fit with a fixed 50:50 ratio of Lorentzian–Gaussian contribution was used to reproduce the spectral features of CuCl/SBA(2.9) Rxn.
[d] Integrated pre-edge intensity. Intensity equals the height multiplied by the full-width-at-half-maximum. Pre-edge modeled as pseudo-Voigt line shape with a fixed 50:50 ratio of Lorentzian–Gaussian contribution.
[e] Inflection point corresponding to shoulder or peak on rising absorption edge.
[f] Highest energy maximum in the first derivative of the data in the rising edge region.
[g] Coordination charge (η) $= -916.66 + 0.32425\ eV^{-1}$ (Rising edge Inflection Point) [43].

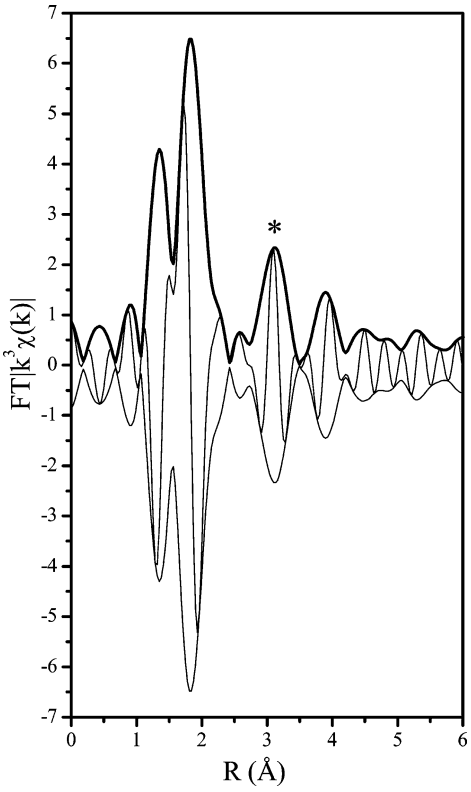

Fig. 8. Cu–Cu phase corrected spectrum of CuCl/SBA(2.9) after reaction conditions at 403 K. Phase correction identifies second nearest neighbor as Cu–Cu scattering component.

with CuCl/SBA(2.9) (1.6(3) and 2.8(3), respectively); however, they were lower than that expected for bulk CuO (4 O nearest neighbors at 1.95 Å, 4 and 8 Cu nearest neighbors at 2.90 and 3.08 Å, respectively). By contrast, CuO^{t}Bu/SBA(3.4) has a noticeable peak at ∼ 2.1 Å and resolvable peaks above 3 Å. Fitting this spectrum reveals a Cu–O contribution and two different Cu–Cu scattering contributions. The Cu–Cu bond distance of 2.54 Å is characteristic of copper metal, and the Cu–O and second Cu–Cu bond distances are more similar to Cu_2O.

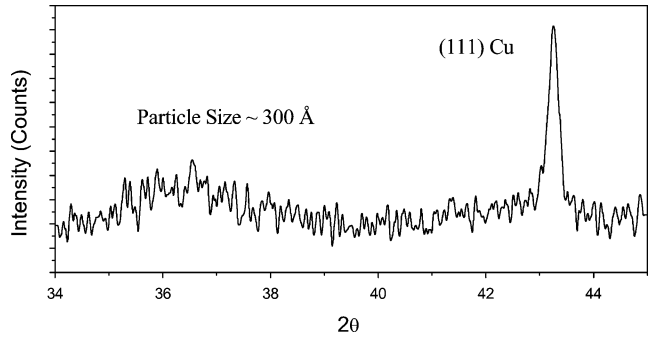

Fig. 9. XRD pattern of Cu/SBA(5.0) after a MeOH/O_2/CO/He gas mixture (4.0/1.0/9.0/19.3) was fed to the reactor at 403 K.

3.3.2. Powder XRD of the catalyst prepared by incipient wetness impregnation

Cu/SBA(5.0) was examined by XRD both before and after exposure to reaction conditions. Following reduction in CO at 573 K, the XRD pattern of Cu/SBA(5.0) exhibits a strong (111) diffraction peak of Cu metal. Following reaction conditions of 20% CO, 2% O_2, and 10% MeOH at 403 K, the XRD pattern of Cu/SBA(5.0) continues to exhibit a (111) diffraction peak of Cu metal (Fig. 9). By Scherrer analysis [61], an upper estimate [62] of the particle size was found to be 300 Å.

4. Discussion

The DMC synthesis activities of various Cu-based catalysts are compared in Table 9. The most active catalyst reported in this communication, CuCl/SBA(2.9), is similar in activity to Cu/X-zeolite [25] and Cu/Y-zeolite [25] at the same temperature and comparable feed compositions. CuCl/SBA(2.9) is nearly three times more active on a total Cu basis compared with CuCl/MCM-41 [21] and similar in activity to $CuCl_2$/a.c. [15]. It is noted, however, that CuCl/MCM-41 and $CuCl_2$/a.c. were tested at CO and MeOH partial pressures higher than those used to test CuCl/SBA(2.9). Increasing the CO and MeOH partial pres-

Table 8
Fitting results for samples after reaction conditions at 403 K

Catalyst	Shell	CN[a]	R[b] (Å)	σ^2[c] (Å^2)	E^0[d] (eV)	ℜ-factor[e]
CuCl/SBA(2.9)	Cu–O	2.8 (3)	1.94 (1)	0.006 (1)	6.1 (1.4)	0.0199
	Cu–Cu	1.6 (3)	2.92 (1)	0.011[f]		
CuOSi/SBA(3.6)	Cu–O	3.4 (2)	1.933 (5)	0.0050 (7)	4.3 (8)	0.0086
	Cu–Cu	2.3 (8)	2.93 (1)	0.011 (2)		
CuO^{t}Bu/SBA(3.4)	Cu–O	2.3 (2)	1.879 (9)	0.004 (1)	3.6 (1.6)	0.0171
	Cu–Cu	0.8 (1)	2.54 (1)	0.008[f]		
	Cu–Cu	1.9 (4)	2.97 (1)	0.012[f]		

[a] Coordination number.
[b] Fitted radial distance.
[c] Debye–Waller factor.
[d] Energy reference shift.
[e] ℜ-factor defined in Experimental section.
[f] Fixed value.

Table 9
DMC productivity comparison to conventional and literature catalysts for vapor phase oxidative carbonylation of methanol

Catalyst	Cu content (wt%)	T (K)	CO (atm)	O_2 (atm)	MeOH (atm)	TOF_{DMC}[a] ($mol_{DMC}\ mol_{Cu}^{-1}\ s^{-1}$) ($\times 10^5$)	Reference
CuCl/SBA(2.9)	2.9	403.0	0.27	0.03	0.12	3.30	This work
$CuCl_2$/a.c.	4.6	393.0	7.60	0.50	1.90	3.10	[15]
CuCl/MCM-41	6.3	403.0	4.40	0.50	0.30	0.85	[21]
Cu/X-Zeolite	30.0	403.0	0.40	0.08	0.20	2.00	[24]
Cu/Y-Zeolite	7.3	403.0	0.46	0.06	0.26	6.80	[25]
Cu/Y-Zeolite/TEAC	12.7	385.0	7.30	0.40	3.60	17.00	[23]

[a] TOF reported on a total Cu basis. Where appropriate, the reported TOF valve was converted to common units based on details in the experimental section of the listed reference.

sures used to evaluate CuCl/SBA(2.9) should have improved its activity, since the kinetics of DMC formation are nearly first order in CO partial pressure [24]. TEAC (tetraethylammonium chloride)-impregnated Cu/Y zeolite is over 5 times more active than CuCl/SBA(2.9) [23]. However, this catalyst was also tested at CO and MeOH partial pressures higher than those used to evaluate CuCl/SBA(2.9). Hence, a part of the higher activity of TEAC-promoted Cu/Y is due to the difference in reaction conditions.

The results presented in Fig. 3 and Table 5 demonstrate that, following He pretreatment at 573 K, the state of Cu dispersion depends more upon the Cu precursor than on the weight loading of Cu below 5.2 wt%. Both atomically dispersed Cu(I) cations and small crystallites of metallic Cu are observed, with the dispersion of Cu decreasing in the order CuCl/SBA $\sim$ CuOSi/SBA $\gg$ CuO^{t}Bu/SBA $\gg$ Cu/SBA(5.0). In all cases, the dispersion of Cu on SBA-15 catalysts prepared by nonaqueous grafting or high-temperature CVD is significantly higher than that which can be achieved by incipient wetness impregnation.

During the oxidative carbonylation of methanol (0.26 atm CO, 0.03 atm O_2, 0.12 atm MeOH, balance He, 403 K), XANES and EXAFS analyses demonstrated that the Cu dispersed on SBA-15 undergoes significant rearrangement. The FT $k^3\chi(k)$ for CuCl/SBA(2.9) and CuOSi/SBA(3.6) are similar in appearance (see Fig. 7). For both catalysts, the bond distances determined by fitting Cu–O and Cu–Cu shells to theoretical standards agree closely with those characteristic of crystalline CuO; however, the absence of Fourier components beyond 3 Å suggests that there is no long-range ordering and, hence, that the CuO is not crystalline. Consistent with this interpretation, the Cu–Cu and Cu–O coordination numbers are lower than those expected for bulk CuO. The XANES analyses of CuCl/SBA(2.9) and CuOSi/SBA(3.6) show evidence for Cu(I) and Cu(II) species. The Cu(I) cations are presumed to lie on the surface of the CuO structures. Helium-pretreated CuO^{t}Bu/SBA(3.4) also undergoes oxidation upon exposure to reaction conditions, but in this case EXAFS and XANES analyses suggest that the small Cu particles become covered with a layer of Cu_2O. In the case of Cu/SBA(5.0), diffraction peaks associated with Cu_2O were not observed. Nevertheless, we believe an overlayer of the large metal particles was similarly passivated by reaction conditions, as shown for CuO^{t}Bu/SBA(3.4) under reaction conditions by EXAFS.

As noted in Figs. 1 and 2 and Table 3, the DMC activity of CuCl/SBA(2.9) is roughly a factor of 2 higher than that of CuOSi/SBA(3.6) on a total Cu basis, but the two catalysts exhibit comparable activities for MF and CO_2. Another striking similarity between these two catalysts is in the values of $S^o_{DMC/MeOH}$ and $S^o_{DMC/CO}$. These are somewhat larger for CuCl/SBA(2.9) versus CuOSi/SBA(3.6) at 403 K, but they become identical at 433 K. The higher DMC activity of CuCl/SBA(2.9) may be due to the promoting effects of Cl on this catalyst. As discussed above, Cl XANES analyses suggest that a portion of the residual Cl in CuCl/SBA(2.9) is associated with Cu. Exactly how Cl would enhance the DMC activity is not understood at this time. Since Cl promotion is known to enhance the DMC synthesis activity of Cu/Y zeolites [23], an effort was made to determine whether an increase in Cl content would further improve the activity of CuCl/SBA(2.9). CH_3Cl was introduced into the reaction mixture as 500-μl pulses. It was determined, however, that at the reaction temperature used CH_3Cl did not dissociate to release Cl. Impregnation of the catalysts with Cl^--containing solutions was not attempted, since it was anticipated that the state of Cu might change during drying and calcination.

It is also notable that the intrinsic DMC selectivity from CO for both catalysts is roughly 50%. This suggests that the synthesis of DMC occurs with the overall stoichiometry shown in reaction (2) and implies that CO_2 is produced concurrently with DMC. A mechanism for such a process has been identified for DMC synthesis from Cu(I) cations exchanged into a zeolite [63]:

$$2CH_3OH + CO + O_2 = (CH_3O)_2CO + CO_2, \quad (2)$$

$$(CH_3O)_2CO + H_2O = 2CH_3OH + CO_2. \quad (3)$$

It is also known that CO_2 can be produced by the hydrolysis of DMC, as shown in reaction (3). To establish whether this reaction might account for CO_2 formation during DMC synthesis, an experiment was performed in which a flow containing 0.01 atm DMC and 0.002 atm H_2O was fed over CuCl/SBA(2.9) at 403 K. Assuming first-order kinetics in DMC and H_2O, the apparent rate constant for the forward reaction was found to be $1.1 \times 10^5\ cm^5\ mol_{Cu}^{-1}\ mol_{DMC}^{-1}\ min^{-1}$.

Although this reaction is rapid, at the concentrations of DMC and H_2O produced during DMC synthesis the rate of DMC hydrolysis is calculated to be too low to account for the additional CO_2 observed. Thus, it appears that the correct stoichiometric reaction for DMC synthesis is reaction (2).

The DMC and MF activities of CuO^{t}Bu/SBA(3.4) are nearly identical to those of CuOSi/SBA(3.6) on a total Cu basis, as is the DMC selectivity from methanol. The significant difference between these catalysts is the much lower DMC selectivity from CO for CuO^{t}Bu/SBA(3.4). Selectivity lower than 50% suggests that CO_2 is produced not only as a by-product of DMC synthesis, but also via CO combustion. The low value of $S^o_{DMC/CO}$ for CuO^{t}Bu/SBA(3.4) is attributed to the presence of Cu_2O in conjunction with Cu. This interpretation is supported by literature reports that show CO combustion activity increases with Cu_2O formation on Cu metal [64–66]. Consistent with this, Table 4 shows that when DMC synthesis is carried out on Cu/SBA(5.0) prepared by aqueous impregnation, the DMC selectivity from CO is very low on a total Cu basis, at the same time that the DMC selectivity from MeOH is comparable to that obtained with CuCl/SBA(2.9).

Thus, the results of the present study indicate that to achieve high DMC activity and selectivity from both MeOH and CO, it is desirable to maintain a high dispersion of Cu and to avoid the formation of Cu crystallites. The preferred active sites for DMC synthesis by oxidative carbonylation appear to be Cu(I) cations dispersed on very small particles of noncrystalline CuO. The activity of these sites is enhanced by the presence of small amounts of Cu–Cl species.

5. Conclusions

$[CuOSi(O^tBu)_3]_4$, $[CuO^tBu]_4$, and CuCl were used as precursors to produce mesoporous silica-supported copper catalysts. XANES and EXAFS characterization prior to reaction showed that Cu in the catalysts prepared with the use of CuCl and $[CuOSi(O^tBu)_3]_4$ was present as isolated Cu(I) cations, whereas use of $[CuO^tBu]_4$ produced 1-nm Cu particles. The state of Cu dispersion depends more upon the Cu precursor than on the weight loading of Cu. Following reaction conditions, EXAFS analysis reveals that CuCl/SBA(2.9) and CuOSi/SBA(3.6) have very similar local Cu environments. Residual Cl is present in CuCl/SBA, and XANES analysis shows that at least some of the Cl is bound to Cu. During reaction, Cu in catalysts prepared from CuCl and $[CuOSi(O^tBu)_3]_4$ formed highly dispersed CuO moieties, whereas the Cu in the catalyst prepared from $[CuO^tBu]_4$ formed a cuprous oxide layer over a Cu(0) core.

High DMC activity correlated with Cu dispersion. The values of $S^o_{DMC/MeOH}$ and $S^o_{DMC/CO}$ decreased with decreasing Cu dispersion when the original state of the Cu was Cu(0).

In conclusion, it was found that:

1. Highly dispersed Cu(I) cations on very small particles of noncrystalline CuO promote $S_{DMC/CO}$, $S_{DMC/MeOH}$, and activity. Although chlorine is not a requirement for DMC production, its presence appears to enhance DMC selectivity.
2. Reduced Cu (in Cu(I) oxide aggregates) promotes increased activity to side reactions producing CO_2.

Acknowledgments

The authors thank S.H. Choi, J. Bronkema, S. Mukhopadhyay, N. Stephenson, B. Wood, Q.T. Liu, M. Zeralla, and Andreas Hyden for their assistance in collecting XAS data at SSRL and NSLS. Dr. F. Schlachter is also recognized for his guidance and support at BL 9.3.1 at the ALS. Portions of this research were carried out at the Stanford Synchrotron Radiation Laboratory, a national user facility operated by Stanford University on behalf of the US Department of Energy, Office of Basic Energy Sciences. Research carried out at the National Synchrotron Light Source, Brookhaven National Laboratory, is supported by the US Department of Energy, Division of Materials Sciences and Division of Chemical Sciences, under Contract No. DE-AC02-98CH10886. This work was supported by the Methane Conversion Cooperative funded by BP and by the Department of Energy under Contract No. DE-AC03-76SF00098.

References

[1] M. A Pacheco, C.L. Marshall, Energy and Fuels 11 (1997) 2.
[2] P. Tundo, M. Selva, Acc. Chem. Res. 35 (2002) 706.
[3] U. Romano, R. Tesel, M.M. Mauri, P. Rebora, Ind. Eng. Chem. Prod. Res. Dev. 19 (1980) 396.
[4] R. Srivastava, D. Srinivas, P. Ratnasamy, Catal. Let. 91 (2003) 133.
[5] T. Wei, M. Wang, W. Wei, Y. Sun, B. Zhong, Green Chemistry 5 (2003) 343.
[6] B.M. Bhanage, S. Fujita, Y. Ikushima, M. Arai, Green Chemistry 5 (2003) 429.
[7] S. Xie, A.T. Bell, Catal. Let. 70 (2000) 137.
[8] K.T. Jung, A.T. Bell, J. Catal. 204 (2001) 339.
[9] K.T. Jung, A.T. Bell, Top. Catal. 20 (2002) 97.
[10] I. Yamanaka, A. Funakawa, K. Otsuka, Chem. Let. (2002) 448.
[11] G. Filardo, A. Galia, F. Rivetti, O. Scialdone, G. Silvestri, Electrochem. Acta 42 (1997) 1961.
[12] G.L. Curnutt, A.D. Harley, in: Oxygen Complexes and Oxygen Activation by Transition Metals, Plenum, New York, 1988, pp. 215–232.
[13] G.L. Curnutt, US Patent, 4,625,044 (1986).
[14] G.L. Curnutt, US Patent, 5,004,827 (1991).
[15] M.S. Han, B.G. Lee, I. Suh, H.S. Kim, B.S. Ahn, S.I. Hong, J. Mol. Catal. A. 170 (2001) 225.
[16] M.S. Han, B.G. Lee, I. Suh, B.S. Ahn, H.S. Kim, D.J. Moon, S.I. Hong, J. Mol. Catal. A. 170 (2003) 137.
[17] K. Tomishige, T. Sakaihori, S. Sakai, K. Fujimoto, Appl. Catal. A. 181 (1999) 95.
[18] H. Itoh, Y. Watanabe, K. Mori, H. Umino, Green Chemistry 5 (2003) 558.
[19] R.X. Jiang, S.F. Wang, X.Q. Zhao, Y.J. Wang, C.F. Zhang, Appl. Catal. A. 238 (2003) 131.

[20] Y. Cao, J.C. Hu, P. Yang, W.L. Dai, K. Fan, Chem. Commun. (2003) 908.
[21] Z. Li, K. Xie, R.C.T. Slade, Appl. Catal. A. 205 (2001) 85.
[22] P. Yang, Y. Cao, J.C. Hu, W.L. Dai, K. Fan, Appl. Catal. A 241 (2003) 363.
[23] D.C. Molzahn, M.E. Jones, G.E. Hartwell, J. Puga, US Patent 5,387,708.
[24] S.A. Anderson, T.W. Root, J. Catal. 217 (2003) 396.
[25] S.T. King, J. Catal. 161 (1996) 530.
[26] S.T. King, Catal. Today 33 (1997) 173.
[27] S.T. King, M.E. Jones, M.M. Olken, US Patent 5,391,803 (1995).
[28] S. Brunauer, P.H. Emmett, E. Teller, J. Am. Chem. Soc. 60 (1938) 309.
[29] E.P. Barrett, L.G. Joyner, P.P. Hakebda, J. Am. Chem. Soc. 73 (1951) 373.
[30] J.A. McGinnety, J. Am. Chem. Soc. 94 (1972) 8406.
[31] M.J. Sharnoff, Chem. Phys. 42 (1965) 3383.
[32] D. Zhao, J. Feng, Q. Huo, N. Melosh, G.H. Fredrickson, B.H. Chmelka, G.D. Stucky, Science 279 (1998) 548.
[33] K.L. Fujdala, T.D. Tilley, J. Am. Chem. Soc. 123 (2001) 10133.
[34] K.W. Terry, C.G. Lugmair, P.K. Gantzel, T.D. Tilley, Chem. Mater. 8 (1996) 274.
[35] T. Tsuda, T. Hashimoto, T. Saegusa, J. Am. Chem. Soc. 94 (1972) 658.
[36] I. Drake, K.L. Fujdala, S. Baxamusa, T.D. Tilley, A.T. Bell, J. Phys. Chem. B, in press.
[37] K.L. Fujdala, I. Drake, T.D. Tilley, A.T. Bell, J. Am. Chem. Soc. 126 (2004) 10864.
[38] R.E. Jentoft, S.E. Deutsch, G.C. Gates, Rev. Sci. Instrum. 67 (1996) 2111.
[39] E.A. Stern, K. Kim, Phys. Rev. B. 23 (1981) 378.
[40] D.C. Koningsberger, R. Prins, X-ray Absorption, Wiley, New York, 1988.
[41] D.C. Koningsberger, B.L. Mojet, G.E. van Dorssen, D.E. Ramaker, Top. Catal. 10 (2000) 143.
[42] B.K. Teo, EXAFS: Basic Principles and Data-analysis, Springer, New York, 1986.
[43] S.E. Shadle, B. Hedman, K.O. Hodgson, E.I. Solomon, Inorg. Chem. 33 (1994) 4235.
[44] B. Hedman, K.O. Hodgson, E.I. Solomon, J. Am. Chem. Soc. 112 (1990) 1543.
[45] B. Hedman, P. Frank, S.F. Gheller, A.L. Roe, W.E. Newton, K.O. Hodgson, J. Am. Chem. Soc. 110 (1988) 3798.
[46] The exact energy position of the pre-edge peak of Cs_2CuCl_4 used in the Cl K-edge calibration of Refs. [31,32] is believed to be based on the S K-edge of 2472.0 eV discussed in Ref. [33].
[47] Personal communication with Fred Schlachter. The rotary encoder was installed as part of recent upgrade to the BL 9.3.1 of the ALS.
[48] T. Ressler, http://ourworld.compuserve.com/homepages/t_ressler/.
[49] T.J. Ressler, Synchrotron Radiat. 5 (1998) 118.
[50] E.A. Stern, M. Newville, B. Ravel, Y. Yacoby, D. Haskel, Physica B 208–209 (1995) 117.
[51] M.J. Newville, Synchrotron Rad. 8 (2001) 322.
[52] IFEFFIT manual: http://cars9.uchicago.edu/ifeffit/.
[53] A.L. Ankudinov, J.J. Rehr, Phys. Rev. B 56 (1997) R1712.
[54] A.L. Ankudinov, C. Bouldin, J.J. Rehr, J. Sims, H. Hung, Phys. Rev. B 65 (2002) 104107.
[55] This statistical value is related to the standard definition of χ^2 but is normalized to the number of degrees of freedom in the fit. The details of this calculation have been described elsewhere; M. Newville, B. Ravel, D. Haskel, J.J. Rehr, E.A. Stern, Y. Yacoby, Physica B 208–209 (1995) 154.
[56] For example, uncalcined: CuOSi/SBA(3.5), 678 $m^2\,g^{-1}$ and 0.88 $cm^3\,g^{-1}$; CuOSi/SBA(5.0), 567 $m^2\,g^{-1}$ and 0.80 $cm^3\,g^{-1}$; CuO^tBu/SBA(5.0), 745 $m^2\,g^{-1}$ and 0.98 $cm^3\,g^{-1}$. After heating: CuOSi/SBA(3.5), 800 $m^2\,g^{-1}$ and 1.01 $cm^3\,g^{-1}$; CuOSi/SBA(5.0), 782 $m^2\,g^{-1}$ and 1.04 $cm^3\,g^{-1}$; and CuO^tBu/SBA(5.0), 813 $m^2\,g^{-1}$ and 1.09 $cm^3\,g^{-1}$.
[57] T. Glaser, B. Hedman, K.O. Hodgson, E. Solomon, Acc. Chem. Res. 33 (2000) 859.
[58] C. Sugiura, T. Suzuki, J. Chem. Phys. 75 (1981) 4357.
[59] C. Sugiura, J. Chem. Phys. 58 (1973) 5444.
[60] P.A. Lee, G. Beni, Phys. Rev. B 15 (1977) 2862.
[61] P. Scherrer, Nachr. Ges. Wiss. Göttinger (1918) 96.
[62] S. Calvin, M.M. Miller, R. Goswami, S.-F. Cheng, S.P. Mulvaney, L.J. Whitman, V.G. Harris, J. Appl. Phys. 94 (2003) 778.
[63] B. Peters, A.T. Bell, Manuscript in preparation.
[64] A. Knop-Gericke, M. Hävecker, Th. Schedel-Niedrig, R. Schlögl, Top. Catal. 15 (2001) 27.
[65] A. Knop-Gericke, M. Hävecker, Th. Schedel-Niedrig, R. Schlögl, Top. Catal. 10 (2000) 187.
[66] G.G. Jernigan, G.A. Somorjai, J. Catal. 147 (1994) 567.